

# Global Contrast Masked Autoencoders Are Powerful Pathological Representation Learners\*

Hao Quan<sup>1</sup>, Xingyu Li<sup>1</sup>, Weixing Chen<sup>2</sup>, Qun Bai<sup>1</sup>, Mingchen Zou<sup>1</sup>, Ruijie Yang<sup>3</sup>, Tingting Zheng<sup>1</sup>, Ruiqun Qi<sup>4</sup>, Xinghua Gao<sup>4</sup>, and Xiaoyu Cui<sup>1</sup>

<sup>1</sup> College of Medicine and Biological Information Engineering, Northeastern University, China

[cuixy@bmie.neu.edu.cn](mailto:cuixy@bmie.neu.edu.cn)

<sup>2</sup> Shenzhen College of Advanced Technology, University of the Chinese Academy of Sciences, Beijing 100049, China

<sup>3</sup> School of Computer Science and Engineering, Northeastern University, China

<sup>4</sup> Department of Dermatology, The First Hospital of China Medical University, China

**Abstract.** Based on digital whole slide scanning technique, artificial intelligence algorithms represented by deep learning have achieved remarkable results in the field of computational pathology. Compared with other medical images such as Computed Tomography (CT) or Magnetic Resonance Imaging (MRI), pathological images are more difficult to annotate, thus there is an extreme lack of data sets that can be used for supervised learning. In this study, a self-supervised learning (SSL) model, Global Contrast Masked Autoencoders (GCMAE), is proposed, which has the ability to represent both global and local domain-specific features of whole slide image (WSI), as well as excellent cross-data transfer ability. The Camelyon16 and NCTCRC datasets are used to evaluate the performance of our model. When dealing with transfer learning tasks with different data sets, the experimental results show that GCMAE has better linear classification accuracy than MAE, which can reach 81.10% and 89.22% respectively. Our method outperforms the previous state-of-the-art algorithm and even surpass supervised learning (improved by 3.86% on NCTCRC data sets). The source code of this paper is publicly available at <https://github.com/StarUniversus/gcmae>

**Keywords:** Self-supervised learning · Pathological image · Representation Learning

## 1 Introduction

Pathology is the gold standard of diagnosis. Traditional pathology mainly focuses on macroscopic observation under microscope. Pathologists determine the nature of lesions and classify tissue based on subjective experience, and the diagnosis results are easily affected by factors such as experience and fatigue [4,11,25]. Computational pathology transforms glass slides into digital images and analyzes with image processing technology, which promotes the transformation of

---

\* H. Quan and X. Li-These authors have contributed equally.

pathological diagnosis from qualitative analysis to quantitative calculation. In recent years, relying on whole slide image scanning technology [19], artificial intelligence algorithms represented by deep learning have achieved remarkable results in the field of computational pathology [4,20,23], and have become a current research hot area and a significant direction of future development of pathology.

Deep learning (DL) is one of the common methods to extract features from computational pathology, which can directly learn sub-visual image features that are difficult for humans to find with eyes [22]. However, most DL methods require a large amount of high-quality labeled data, which are difficult to transfer to other data sets with different feature spaces or probability distribution functions [1]. Different staining methods, scanning equipment, different diseases and intra-class differences across organs and tissues will lead to data feature differences and long tail problems especially in the field of computational pathology [22]. Maximizing the use of source domain data sets for representation learning becomes an important method to alleviate the poor performance of the model caused by data scarcity in the target domain [1,28,17].

Recently, self-supervised visual representation learning has achieved great success in the field of natural images [13,5,6,12,7,2,8,14]. SSL can use proxy tasks to mine valuable representation information from large-scale unsupervised data. In the past two years, researchers have applied SimCLR [5], MoCo [13] and other SSL methods based on contrastive learning to computational pathology, and transferred the pre-training model to downstream tasks, which can narrow down the accuracy gap between unsupervised learning and supervised learning [9]. In addition, some researchers designed reasonable data augmentation methods and complex proxy tasks to expand the representation space of pathological images according to the characteristics of pathological images. Yang et al. [27] designed a cross-stain prediction and a new data augmentation method stain vector perturbation based on the characteristics of pathological images, and proposed CS-CO method based on contrastive learning, which verified its effectiveness on NCTCRC data sets; Li et al. [21] developed SSLP method, which mines pathological features from three aspects: self-invariance, intra-invariance and inter-invariance by designing complex proxy tasks, and surpasses supervised method on camelyon16 data set. However, the above-mentioned self-supervised method based on contrastive learning has the problems of large consumption of hardware resources, difficulty in training multi-task learning, and lower performance of cross-data set transfer learning than supervised learning [14,24]. Therefore, simplifying proxy tasks and enhancing general representation ability are the key problems to be solved in pathological representation learning.

In 2021, as an extensible SSL method, Mask Autoencoder (MAE) achieved SOTA results in ImageNet dataset [14]. This method randomly masks part of the input image and uses the lightweight decoder to rebuild the obscured pixels, which can not only improve the accuracy but also speed up the training, and the learning efficiency is better than that of contrastive learning [14]. Pathological diagnosis often needs to consider both global and local features of WSIs [4]. Due

to the morphological similarity of cells and tissues of the same type, MAE may have the potential to find the correlation within pathological image tile, that is, to extract local features. Correspondingly, if we use the memory bank structure [26] of contrast learning to store the features between each tile, such MAE may also have the ability to obtain global features.

Based on the above analysis, we proposed a Global Contrast Mask Autoencoder (GCMAE) SSL model that can extract both global and local features from pathological images. On one hand, based on MAE network structure, the model can obtain the internal hidden space feature representation of each patch in pathological images. On the other hand, the model integrates memory bank structure to store global features of pathological images, contrastive learning is used to mine feature associations between tiles. The main contributions of this study are as follows:

1. First application of MAE self-supervised neural network architecture to the field of WSI characterization and analysis of mask ratio for pathological images, providing guidance for subsequent research;
2. To propose the GCMAE self-supervised neural network model for WSI analysis, which has the ability to characterize global features and local features simultaneously and has stronger cross-dataset characterization capability compared to MAE.

Experimental results show that the method proposed in this study has advantages in generic representation and downstream cross-disease transfer learning tasks, outperforming supervised learning and MAE on pathological image classification tasks.

## 2 Method

Figure 1 shows the overall framework of our proposed GCMAE SSL algorithm, which is assisted by two proxy tasks: image reconstruction and contrastive learning. A group of unlabeled pathological image tiles are extracted during the pre-processing. Then each tile is cut into 16\*16 patches, and part of the patches are randomly masked. The visible patches are input into encoder and mapped into latent representation, which is also momentum updated to the memory bank at the same time. In our framework, the image reconstruction proxy task is implemented by the MAE network, which can extract the visual features of tiles, while the proxy task of contrastive learning can improve the general representation ability of MAE algorithm for pathological images. As shown in Eq.(1), the weighted sum of the MSE loss [14] of tile feature extraction and the NCE loss [26] of global feature extraction is used as the cost function, which can reduce the distance between similar features while learning the high-level features of images, so as to improve the generalization of the model and improve the accuracy of the cross-dataset transfer learning task.

$$\mathcal{L} = \lambda_1 \mathcal{L}_{MSE} + \lambda_2 \mathcal{L}_{NCE} \quad (1)$$

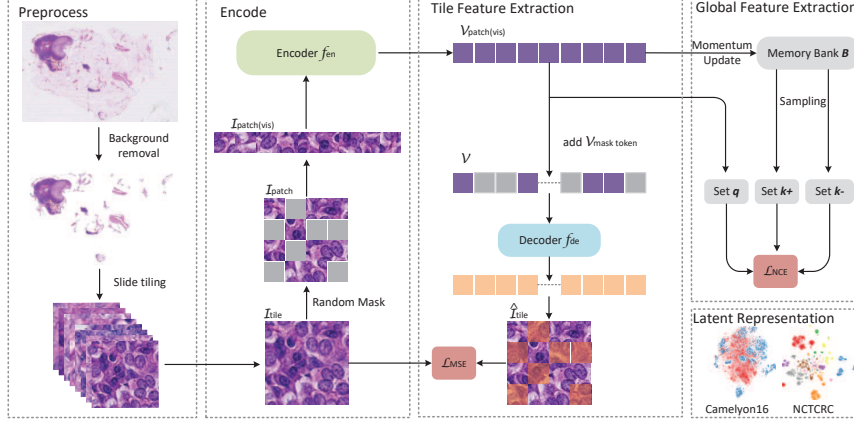


**Fig. 1.** Framework of GCMAE, tile feature extraction is the proxy task of image reconstruction, while global feature extraction is the proxy task of contrastive learning. The latent representation is the t-SNE result of encoder output.

## 2.1 Encoder

The vision transformer (ViT) [10] is regarded as encoder backbone  $f_{en}$ . Firstly,  $224 * 224$  tiles  $\mathcal{I}_{tile}$  are divided into regular non overlapping patches ( $16 * 16$ )  $\mathcal{I}_{patch}$ ; Then, the patch is randomly sampled by uniform distribution to mask some patches, and the visible parts form a new subset of patches  $\mathcal{I}_{patch(vis)}$ . The image features of the visible parts are embedded by linear projection and the position information is encoded by positional embeddings, where position embedding is implemented by standard learnable 1D vectors. The embedded features and position information are fed into the transformer block to extract a latent representation of the visible parts of the tile.

## 2.2 Tile Feature Extraction

As a decoder  $f_{de}$ , tile feature extraction consists of eight transformer blocks. In addition to the latent representation  $\mathcal{V}_{patch(vis)}$ , which is used to indicate the missing patch. The mask token also contains the position embedding of all patches, which is used to reconstruct the missing pixels. The normalized tiles are used as the target to calculate the MSE loss, Eq. (4). The random sampling strategy of the tiles can remove redundant information and realize the difficult proxy task that can not directly reconstruct the original missing pixels from adjacent patches. However, it can only represent the internal features of each tile, but can not represent the feature relationship between different tiles.

$$\mathcal{V} = f_{en}(\mathcal{I}_{patch(vis)}) + \mathcal{V}_{mask-token} \quad (2)$$

$$\hat{\mathcal{I}}_{tile} = f_{de}(\mathcal{V}) \quad (3)$$

$$\mathcal{L}_{MSE} = \frac{1}{n} \sum_{i=1}^n (\mathcal{I}_{tile} - \hat{\mathcal{I}}_{tile})^2 \quad (4)$$

### 2.3 Global Feature Extraction

Global feature extraction is implemented through contrastive learning [26]. The latent representation  $V_{patch(vis)}$  is not only inputted to the decoder for image reconstruction, but also updated to memory bank  $\mathbf{B}$  with a momentum coefficient  $\tau$  for storing global features. We have designed the momentum update feature in a different way to the momentum update model parameters in MoCo, using only a separate encoder and memory bank to enable contrastive learning. Specifically, it is known that the latent representation at the output of the current epoch encoder is  $V_{patch(vis)}$  and the latent representation deposited in  $\mathbf{B}$  from the previous epoch is  $V'_{patch(vis)B}$ . The latent representation  $V_{patch(vis)B}$  deposited in  $\mathbf{B}$  from the current epoch is

$$V_{patch(vis)B} = \frac{0.5V_{patch(vis)} + 0.5V'_{patch(vis)B}}{\|0.5V_{patch(vis)} + 0.5V'_{patch(vis)B}\|^2} \quad (5)$$

The main reason for this design  $V_{patch(vis)B}$  is twofold: 1. it can alleviate the differences in features of the same sample in different epochs caused by different model parameters and random masks during the training process of the network. 2. Combining adjacent epoch features can construct pathological feature representations with higher information density, thus improving the generic feature representation capability of GCMAE.

We construct  $V_{patch(vis)B}$  as a dictionary to be stored as a data sample queue in  $\mathbf{B}$ . The  $V_{patch(vis)B}$  corresponding to the current epoch input mini-batch is extracted from  $\mathbf{B}$  as the key value  $k^+$ . The current mini-batch of  $V_{patch(vis)}$  as query  $q$  forms a positive pair with  $k$ . The potential features of  $n$  samples drawn randomly from the memory bank form a negative pair with  $q$ . Cosine similarity is used as a means of evaluating the distance between features to calculate the similarity between  $V_{patch(vis)}$ . We consider an efficient form of the contrast learning loss function, called infoNCE, to minimize the distance between positive pairs and maximize the distance between negative pairs, with the loss function defined as follows.

$$\mathcal{L}_{q,k^+,B} = -\log \frac{\exp(q^T k^+ / \tau)}{\exp(q^T k^+ / \tau) + \sum_{k^- \in B} \exp(q^T k^- / \tau)} \quad (6)$$

$\tau$  is a temperature parameter that controls the concentration level of the distribution [15].

### 3 Experimental Results

#### 3.1 Dataset

Two pathological data sets were used to evaluate the GCMAE algorithm performance:

1. Camelyon16: The Camelyon16 Challenge dataset contained a total of 400 sentinel lymph node WSIs. The number of pixels contained in these WSIs is roughly the same as that of the entire ImageNet data set [4]. Similar to literature [21], we randomly cut 270,000 tiles from normal and tumor tissues;
2. NCTCRC: NCTCRC dataset comes from the non-overlapping tile of HE stained tissue images of human colorectal cancer and normal tissues, in which the training set contains 100,000 images and the test set contains 7,180 images..

All images are 224\*224 Pixels (PX) at 0.5 microns per pixel (MPP). The details of the data set can be found in Appendix A in the supplementary material.

#### 3.2 Implementation Details

Following [14], the hyper-parameters of GCMAE method are set:  $\tau = 0.07$ ,  $t = 0.5$ ,  $k^- = 8192$ , epochs = 80. With regard to the loss function, it is confirmed by experiments that  $\lambda_1 = 1$  and  $\lambda_2 = 0.1$  can ensure that the loss values of MSE and NCE are in the same order of magnitude. The optimizer is AdamW, betas= (0.9, 0.95). Other hyper-parameters are consistent with those in MAE. Compared to CNNs with inductive bias, ViT as a large model has stronger generalization ability, which is conducive to the construction of generic representation models in the field of pathology. Thus, we use vit-base (ViT-B/16) as the supervised learning benchmark model and the backbone of MAE and GCMAE. See Appendix B of supplementary materials for details of hyper-parameters setting of downstream tasks and comparison methods. In order to alleviate the influence of over-fitting on the representation ability of SSL model, we determined that epochs=80 is suitable for the current data scale through pre-experiment. All SSL experiments below follow this setting. See Appendix C of supplementary materials for details of pre-experiment. All self-supervised pre-training experiments do not use any labels, and all experiments are trained on RTX A6000 GPU.

#### 3.3 Mask Ratio

Table 1 shows the effect of mask ratio on pathological representation of MAE. In the application of pathological representation, 50% mask ratio is suitable for linear classification and 80% mask ratio is suitable for fine-tuning, which is in contrast to the optimal mask ratio of 75% in natural image application. Pathological images contain abundant tissue features and their information density is higher than that of natural images. Therefore, when using MAE model to reconstruct pathological images, more information needs to be known. However,

the optimal result of model fine-tuning is achieved at a higher mask ratio of 80%, which shows that the mask ratio suitable for linear classification in pathological image field is not suitable for model fine-tuning, which further proves the result in [14]. Consistent with the results of natural images, the influence of pre-training models with different mask ratios on model fine-tuning is lower than that of linear classification, and the verification accuracy of model fine-tuning is basically better than that of supervised learning, only slightly lower than that of supervised learning at 90%.

**Table 1.** different mask ratio in WSIs.

		10%	20%	30%	40%	50%	60%	70%	75%	80%	90%
Linear Prob	Acc. (%)	80.98	81.85	82.03	82.29	<b>85.17</b>	81.91	82.16	81.33	80.60	81.11
	AUC (%)	89.86	90.34	90.62	91.08	<b>93.02</b>	90.51	90.59	89.08	88.13	87.38
Fine Tune	Acc. (%)	83.61	83.16	83.34	83.38	82.82	83.33	82.95	83.83	<b>84.95</b>	83.98
	AUC (%)	92.91	92.10	92.27	92.47	92.70	92.23	92.23	92.35	<b>93.43</b>	92.72

### 3.4 Linear Classification

We used the Camelyon 16 dataset to evaluate the linear classification performance of MAE, GCMAE, and other state-of-the-art methods, as shown in Table 3. Experimental results show that the accuracy of SSLP, MAE and GCMAE surpass supervised learning by 1.7%, 3.97% and 2.09%, respectively, and MAE is the best. The GCMAE and MAE methods benefit from a mask ratio strategy where only 50% of the full dataset is visible at each epoch, which is a significant efficiency gain compared to comparative learning where at least 200% of the data is visible (data augmentation).

**Table 2.** Linear classification results of different methods on camelyon16 data set. Both MOCO v1 and MOCO v2 encoders use ResNet50 [16] to extract features and output 512-dimensional feature representation. The data set used by SSLP method is consistent with that of this study, so we directly refer to the experimental results of SSLP in the table. Inside parentheses are performance improvements compared to the supervised method benchmark..

Method	Acc. (%)	AUC (%)
Supervised learning (ViT) [10]	81.20	89.76
MoCo v1 (k = 4096) [13]	70.06	77.79
MoCo v2 (k = 65536) [6]	74.61	86.39
SSLP [21]	82.90(+1.7)	85.70(-4.06)
MAE [14]	<b>85.17(+3.97)</b>	<b>93.02(+3.26)</b>
GCMAE (ours)	83.29(+2.09)	89.82(+0.06)

In this task, the linear classification results of GCMAE were weaker than those of MAE. Specifically, GCMAE used a strategy of momentum update features to construct pathological representations with higher information density by combining features of different levels, thus improving the pathological generic representation capability. However, this reduces the feature consistency constraint on this dataset. This may be the reason why GCMAE is less accurate than MAE on the linear classification task on this dataset. However, in the next cross-dataset migration learning task, GCMAE will outperform the MAE method across the board, reflecting the advantages of the momentum update feature strategy.

### 3.5 Cross-Dataset Transfer Learning

We compared the pathological general visual representation ability of supervised learning, MAE and GCMAE by transferring learning tasks across datasets and diseases, and still used linear classification downstream task evaluation. We use MAE and GCMAE methods to do SSL on camelyon16 and NCTCRC respectively, and obtain four sets of pre-training parameters: MAE(camelyon), MAE(nctcrc), GCMAE(camelyon) and GCMAE(nctcrc), and then transfer the pre-training parameters across datasets to do downstream tasks of linear classification. The experimental results are shown in the '100%' section of Table 4. In the above two cross-dataset tasks, the linear classification accuracy of GCMAE outperforms that of MAE. On camelyon16 dataset, the accuracy of GCMAE method is only 0.1% lower than that of supervised learning method. On NCTCRC dataset, GCMAE method, with an increase of 7.32%, surpasses supervised learning method. This shows that GCMAE has stronger general visual representation ability, and GCMAE can be used as a more effective method to obtain pre-training parameters in cross-disease transfer learning tasks.

**Table 3.** GCMAE and MAE methods transfer learning performance across data sets. '100%' means using the entire training set, and '10%' means using 10% of the data in the entire training set. In parentheses are performance improvements compared to supervised benchmarks.

Dataset	Pretraining Parameter	Acc. (%)	AUC (%)
Camelyon(100%)	Supervised learning(vit)	<b>81.20</b>	89.76
	MAE(nctcrc)	80.88(-0.32)	89.15(-0.61)
	GCMAE(nctcrc)	81.10 (-0.1)	<b>90.03 (+0.27)</b>
NCTCRC(100%)	Supervised learning (vit)	81.90	97.76
	MAE(camelyon)	85.36(+3.46)	98.36(+0.6)
	GCMAE(camelyon)	<b>89.22 (+7.32)</b>	<b>98.74 (+0.98)</b>
Camelyon(10%)	MAE(nctcrc)	79.55(-1.65)	87.68(-2.08)
	GCMAE(nctcrc)	<b>79.89(-1.31)</b>	<b>88.52(-1.24)</b>
NCTCRC(10%)	MAE(camelyon)	84.6(+2.7)	97.99(+0.23)
	GCMAE(camelyon)	<b>86.69(+4.79)</b>	<b>98.10(+0.34)</b>

In order to further verify the ability of GCMAE to extract general visual representations, we randomly selected 10% of the data from the training sets of two data sets for the downstream task of linear classification. The experimental results are shown in the '10%' section of Table 4. On the NCTCRC dataset, our method can still surpass MAE method and supervised method trained with entire data sets by 1.33% and 4.79%, respectively, using only 10% labeled data and linear classifier, which proves that our method has the potential to transfer to few-shot learning tasks and is of great help to build a model for rare disease analysis.

#### 4 Conclusion

In this paper, the Global Contrast Mask Autoencoder (GCMAE), a self-supervised learning method is proposed, which improves MAE's general representation ability by introducing contrastive learning, and achieves state-of-the-art methods in cross-dataset transfer learning linear classification task, even surpassing supervised learning. It is expected to alleviate the influence of medical image long tail problem on the model through cross-dataset pre-training. Secondly, we discuss mask ratio, which is suitable for pathological characterization, and find that MAE is also superior to the most advanced methods in self-supervised linear classification of pathological images. In the future work, we will further optimize the GCMAE method according to the characteristics of pathological images, and transfer the representations obtained by this method to the downstream task of disease prediction with few-shot learning at WSI level.

**Acknowledgement** This work is supported by the National Natural Science Foundation of China (Nos.82072095).

## References

1. Agarwal, N., Sondhi, A., Chopra, K., & Singh, G.: Transfer learning: Survey and classification. In: Smart innovations in communication and computational sciences, pp. 145-155. Springer, Singapore (2021).
2. Bao H., Dong L., Wei F.: Beit: Bert pre-training of image transformers. arXiv preprint arXiv:2106.08254 (2021).
3. Bejnordi, B.E., et al.: Diagnostic assessment of deep learning algorithms for detection of lymph node metastases in women with breast cancer. *JAMA* **318**(22), 2199–2210 (2017)
4. Campanella, G., Hanna, M.G., Geneslaw, L. et al.: Clinical-grade computational pathology using weakly supervised deep learning on whole slide images. *Nat Med* **25**(8), 1301–1309 (2019). <https://doi.org/10.1038/s41591-019-0508-1>
5. Chen T., Kornblith S., Norouzi M., et al.: A simple framework for contrastive learning of visual representations. In: International conference on machine learning. pp. 1597-1607 (2020).
6. Chen X., Fan H., Girshick R., et al.: Improved baselines with momentum contrastive learning. arXiv preprint arXiv:2003.04297 (2020).
7. Caron M., Misra I., Mairal J., et al.: Unsupervised learning of visual features by contrasting cluster assignments. *Advances in Neural Information Processing Systems*, **33**, 9912-9924 (2020).
8. Chen M., Radford A., Child R., et al.: Generative pretraining from pixels. In: International Conference on Machine Learning. PMLR, pp. 1691-1703 (2020).
9. Dehaene O., Camara A., Moindrot O., et al.: Self-supervision closes the gap between weak and strong supervision in histology. arXiv preprint arXiv:2012.03583 (2020).
10. Dosovitskiy A., Beyer L., Kolesnikov A., et al.: An image is worth 16x16 words: Transformers for image recognition at scale. arXiv preprint arXiv:2010.11929 (2020).
11. Elmore J.G., Longton G.M., Carney P.A., et al.: Diagnostic Concordance Among Pathologists Interpreting Breast Biopsy Specimens. *JAMA* **313**(11), 1122–1132 (2015).
12. Grill J. B., Strub F., Altché F., et al.: Bootstrap your own latent-a new approach to self-supervised learning. *Advances in Neural Information Processing Systems*, **33**, 21271-21284 (2020).
13. He K., Fan H., Wu Y., et al.: Momentum contrast for unsupervised visual representation learning. In: Proceedings of the IEEE/CVF conference on computer vision and pattern recognition. pp. 9729-9738 (2020).
14. He K., Chen X., Xie S., et al.: Masked autoencoders are scalable vision learners. arXiv preprint arXiv:2111.06377 (2021).
15. Hinton G., Vinyals O., Dean J.: Distilling the knowledge in a neural network. arXiv preprint arXiv:1503.02531 (2015).
16. He K., Zhang X., Ren S., et al.: Deep residual learning for image recognition. In: Proceedings of the IEEE conference on computer vision and pattern recognition. pp. 770-778 (2015).
17. Kolesnikov A., Beyer L., Zhai X., et al.: Big transfer (bit): General visual representation learning. In: European conference on computer vision. Springer, Cham, pp. 491-507 (2020).
18. Kather, J.N., Halama, N., Marx, A.: 100,000 histological images of human colorectal cancer and healthy tissue. <https://doi.org/10.5281/zenodo.1214456>
19. Litjens G., Kooi T., Bejnordi B. E., et al.: A survey on deep learning in medical image analysis. *Medical image analysis* **42**, 60-88 (2017).

20. Lu M. Y., Williamson D. F. K., Chen T. Y., et al.: Data-efficient and weakly supervised computational pathology on whole-slide images. *Nature biomedical engineering* **5**(6), 555-570 (2021).
21. Li J., Lin T., Xu Y.: SSLP: Spatial Guided Self-supervised Learning on Pathological Images. In: *International Conference on Medical Image Computing and Computer-Assisted Intervention*. Springer, Cham, pp. 3-12 (2021).
22. Pati P., Foncubierta-Rodríguez A., Goksel O., et al.: Reducing annotation effort in digital pathology: A Co-Representation learning framework for classification tasks. *Medical Image Analysis* **67**, 101859 (2021).
23. Quan H., Xu X., Zheng T., et al.: DenseCapsNet: Detection of COVID-19 from X-ray images using a capsule neural network. *Computers in biology and medicine* **133**, 104399 (2021).
24. Ruder S.: An overview of multi-task learning in deep neural networks. *arXiv preprint arXiv:1706.05098* (2017).
25. Wang D., Khosla A., Gargya R., et al.: Deep learning for identifying metastatic breast cancer. *arXiv preprint arXiv:1606.05718* (2016).
26. Wu Z., Xiong Y., Yu S. X., et al.: Unsupervised feature learning via non-parametric instance discrimination. In: *Proceedings of the IEEE conference on computer vision and pattern recognition*. pp. 3733-3742 (2018).
27. Yang P., Hong Z., Yin X., et al.: Self-supervised visual representation learning for histopathological images. In: *International Conference on Medical Image Computing and Computer-Assisted Intervention*. Springer, Cham, pp. 47-57 (2021).
28. Zhuang F., Cheng X., Luo P., et al.: Supervised representation learning: Transfer learning with deep autoencoders. In: *24th International Joint Conference on Artificial Intelligence*, pp. 4119-4125. Buenos Aires (2015).

## 5 Appendix

### 5.1 Dataset Details

Table A: Details of datasets. The Camelyon 16 dataset distribution is based on SSLP settings, but the data size is one-third of that of SSLP. NCTCRC is a complete NCT-CRC-HE-100K data set.

Data	Task	normal patch	tumor patch	overall
Camelyon	Pretraining	200,000	20,000	220,000
	Train	20,000	20,000	40,000
	Test	5,000	5,000	10,000
NCTCRC	Pretraining	-	-	100,000
	Train	-	-	100,000
	Test	-	-	7,180

### 5.2 Implementation Details

Table B: Details of the implementation of the experiment. The details not presented in Table B are consistent with those in the corresponding papers of this method, so please refer to the references.

	backbone	Batch size	epochs	warmup_epochs	norm_pix_loss
Supervised learning	ViT-B/16	128	90	10	-
MoCo v1	ResNet50	128	80	-	-
MoCo v2	ResNet50	128	80	-	-
MAE	ViT-B/16	128	80	5	True
GCMAE	ViT-B/16	128	80	40	False
Linear Classification	ViT-B/16	512	90	10	-
Fine Tune	ViT-B/16	128	50	5	-

### 5.3 Pre-experiment

In order to mitigate the influence of over-fitting on the representation ability of the model, we set the epochs of MAE algorithm no less than 120 times. We use linear classification as a downstream task to evaluate the representational ability of the model. According to Table C, when epochs = 80, the verification accuracy reaches the optimum, and then the accuracy decreases and over-fitting occurs.

Table C: Performance of models saved by different epochs in linear classification tasks. Epochs = 80, the accuracy is the best.

epoch	40	60	80	100	120
Acc. (%)	80.08	80.63	<b>81.33</b>	80.02	78.72
AUC(%)	88.79	89.00	<b>89.08</b>	88.95	87.27